Geophys. J. Int. (2006) **165,** 485–500 doi: 10.1111/j.1365-246X.2006.02856.x

Time-lapse traveltime change of singly scattered acoustic waves

C. Pacheco and R. Snieder*

Center for Wave Phenomena, Department of Geophysics, Colorado School of Mines, Golden, CO, 80401, *USA. E-mail: cpacheco@mines.edu*

Accepted 2005 October 24. Received 2005 October 21; in original form 2005 July 28

SUMMARY

We present a technique based on the single-scattering approximation that relates time-lapse localized changes in the propagation velocity to changes in the traveltime of singly scattered waves. We describe wave propagation in a random medium with homogeneous statistical properties as a single-scattering process where the fluctuations of the velocity with respect to the background velocity are assumed to be weak. This corresponds to one of two end-member regimes of wave propagation in a random medium, the first being single scattering, and the second multiple scattering. We present a formulation that relates the change in the traveltime of the scattered waves to a localized change in the propagation velocity by means of the Born approximation for the scattered wavefield. We validate the methodology with synthetic seismograms calculated with finite differences for 2-D acoustic waves. Potential applications of this technique include non-destructive evaluation of heterogeneous materials and time-lapse monitoring of heterogeneous reservoirs.

Key words: Born approximation, random media, scattering.

1 INTRODUCTION

In the search for technically simple and computationally inexpensive methods for monitoring the time varying behaviour of the subsurface, such as changes associated with a producing hydrocarbon reservoir, we consider coda wave methods to be promising because of their great sensitivity to small changes in the medium. Here we explore the time-lapse behaviour of singly scattered acoustic waves under localized changes in the propagation velocity of the medium.

Coda waves are the result of the interaction of an incident wave with the heterogeneities of the medium that gives rise to scattered waves. Many studies have described these scattered waves as multiply scattered waves, and the diffusion approximation has been employed to characterize the energy transport in strongly scattering media (Aki & Chouet 1975; Turner & Weaver 1994; Page *et al.* 1995; Schriemer *et al.* 1997). In particular, multiply scattered waves have been used to monitor temporal changes in the medium due to the high sensitivity of these waves to small changes in the medium (Weitz & Pine 1993; Yodh & Chance 1995; Snieder *et al.* 2002; Jian *et al.* 2003). Recently, Pacheco & Snieder (2005) use the diffusion approximation to account for the traveltime change of multiply scattered waves due to a localized velocity perturbation.

There are many important practical applications where scattering is not sufficiently strong for the diffusion approximation to be used to model the energy propagation in the scattering medium. Seismic imaging techniques, as used in oil exploration (Claerbout 1985), rely on the single-scattering approximation to obtain an image of the subsurface. In the single-scattering model all scattered waves are assumed to have been scattered once on their way from the source to the receiver, this is usually called the first Born approximation. The application of this approximation to coda waves is valid for weakly scattering media. The Born approximation has been used in theoretical studies of the apparent attenuation of a scattering medium (Chernov 1960; Wu 1982) and in the analysis of the decay of the coda envelope for microearthquakes (Aki & Chouet 1975; Sato 1977). Kopnichev (1977) calculated the time dependence of the energy of the seismogram's coda by applying the Born approximation to scattering theory.

Leary (2002) used first-order elastic wave scattering theory to numerically simulate time-lapse borehole seismic data aimed at monitoring oil–water substitution in heterogeneous hydrocarbon reservoirs. In his work, *P*-wave backscatter 'snapshots' of a heterogeneous rock can be acquired with a borehole seismic source and sensor located at the centre of the volume. Using this methodology, Leary (2002) was able to image the large-scale time-lapse variations of the scattering volume that are the essential drainage structures that a reservoir model incorporates.

*Pacific Region Office, GJI.

Here we consider the time-lapse variation of the traveltime of the scattered waves caused by a localized slowness perturbation. We restrict ourselves to singly scattered waves. The case of multiply scattered waves, investigated in Pacheco & Snieder (2005), relies on a different diffusion approximation for the scattered wavefield. A small change in the propagation velocity of the medium induces a change in the traveltime of the perturbed wavefield with respect to the unperturbed wavefield. The difference in the time of propagation between the unperturbed and perturbed scattered waves provides a framework to estimate changes in the propagation velocity of finite extent. In this work we determine the mean traveltime change of the scattered wavefield for a given localized propagation velocity perturbation.

The remainder of this paper is divided into five parts. In Section 2 we introduce coda wave interferometry and explain how to obtain an estimate of the mean traveltime change of waves by cross-correlating the unperturbed and perturbed wavefields. Section 3 reviews the single-scattering model and how to numerically simulate singly scattered waves. In Section 4 we present a theory that accounts for the time-lapse variation of the traveltime of the scattered waves using the single-scattering approximation. With this technique we calculate the mean traveltime change for any given source–receiver pair due to localized perturbation in the propagation velocity. For the sake of simplicity, the theory has been developed for 2-D acoustic waves. We validate this theory in Section 5 by computing the unperturbed and perturbed seismograms with the aid of a fourth-order finite-difference algorithm and measure the change in the traveltime of the wavefield for different source and receiver pairs, and compare this with the theoretical traveltime change that is derived in this paper. Finally in Section 6 we discuss applications and possible limitations of this technique.

2 CODA WAVE INTERFEROMETRY

In order to find the imprint of localized velocity changes in the scattering medium, we derive an expression that relates the traveltime change with the localized slowness perturbation in the medium. Snieder *et al.* (2002), using the technique called coda wave interferometry, were able to detect temperature dependent changes in the velocity of a granite sample by measuring the difference in the traveltime of scattered waves at different times. For a weak perturbation in the slowness, estimates of small velocity perturbations can be obtained from the unperturbed and perturbed waves by a time-windowed cross-correlation of the scattered waves recorded before and after the perturbation. The unperturbed wavefield $u_u(t)$ can be written as a summation of waves over all possible scattering paths P (Snieder 1999)

$$u_u(t) = \sum_P A_P(t), \tag{1}$$

where for single scattering the paths P are defined by ellipses as shown in Fig. 1. The possible locations for scatterers are distributed on the ellipses. Scattered energy (centre and right panels) arrives after the first or direct arrival (left panel). Notice that for a given traveltime t, energy arriving at the receiver is the sum of waves that have been scattered at different locations on the single-scattering ellipse. It is convenient, therefore, to define a quantity called the mean traveltime change $\langle\tau\rangle(t)$ that represents the average traveltime difference between all the unperturbed and perturbed waves that arrive at the receiver within a time window $(t - t_w, t + t_w)$.

When we introduce a small perturbation of the propagation velocity, the effect of this perturbation on the geometrical spreading and the scattering strength can be ignored (Snieder 2006), and the dominant effect on the waveform arises from the change in the traveltime of the

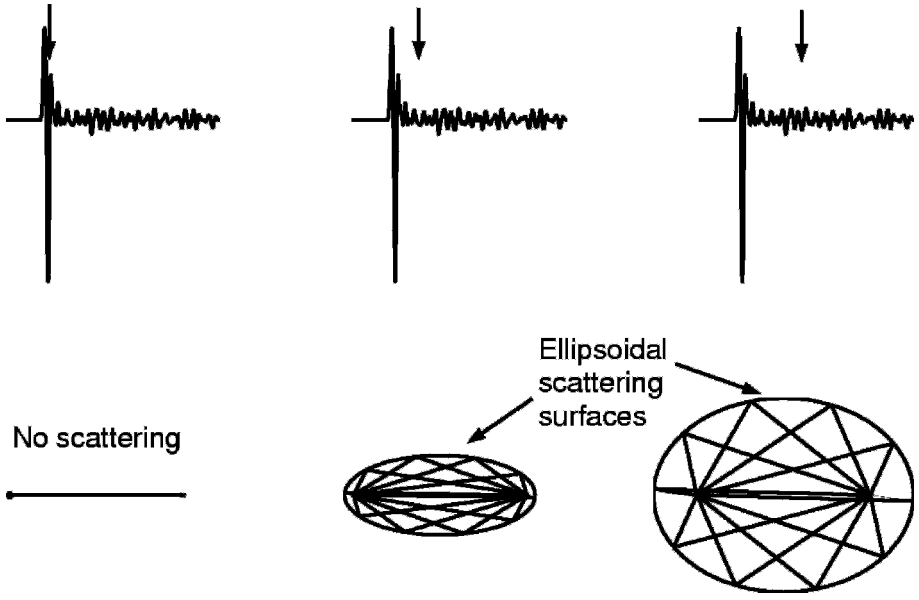

Figure 1. Single-scattering paths for different propagation times t. Top: seismogram indicating three energy arrival times. Bottom: single-scattering ellipses and ray paths for the three arrival times indicated on the seismogram.

wave that travels along each path:

$$u_p(t) = \sum_P A_P(t - \tau_P), \tag{2}$$

where τ_P is the traveltime perturbation for the propagation along trajectory P due to the slowness perturbation. Snieder *et al.* (2002) characterized the change in the wavefield using the time-windowed cross-correlation function, defined as

$$C_{\rm up}^{(t,t_w)}(t_s) = \int_{t-t_w}^{t+t_w} u_u(t')u_p(t'+t_s)\,dt', \tag{3}$$

where t denotes the centre of a time window of length $2t_w$, and t_s is the lag time for the correlation. When eqs (1) and (2) are inserted into eq. (3), double sums $\sum_{PP'}$ appear. We assume that in these double sums, the cross terms related to different paths ($P \neq P'$) are incoherent and average out to zero when the mean of the source signal vanishes. The contribution of the crossterms is estimated by Snieder (2004). A dimensionless measure of the change of the wavefield is given by the time-windowed correlation coefficient, which is given by

$$R^{(t,t_w)}(t_s) = \frac{\int_{t-t_w}^{t+t_w} u_u(t')u_p(t'+t_s)\,dt'}{\left(\int_{t-t_w}^{t+t_w} u_u^2(t')\,dt' \int_{t-t_w}^{t+t_w} u_p^2(t')\,dt'\right)^{1/2}}. \tag{4}$$

For time shifts t_s much smaller than the dominant period T of the wave, a second-order Taylor expansion of the wave field in τ_P gives (Snieder 2006)

$$R^{(t,t_w)}(t_s) = 1 - \frac{1}{2}\bar{\omega}^2\langle(\tau_P - t_s)\rangle^2(t, t_w), \tag{5}$$

where $\bar{\omega}$ is the dominant frequency of the wave. In this expression $\langle ...\rangle_{(t,t_w)}$ denotes the average over all waves that arrive in the time window $(t - t_w, t + t_w)$ with a weight factor that is equal to the intensity of the waves (Snieder 2006). Thus, averages are taken with a weight factor that is given by the intensity of each singly scattered wave. This means that in this work, the average traveltime change $\langle\tau\rangle(t, t_w)$ is given by an average of the traveltime change of individual waves with different paths P arriving on the time window $(t - t_w, t + t_w)$, that is,

$$\langle\tau\rangle(t, t_w) = \frac{\sum_P w_P(t, t_w)\tau_P(t, t_w)}{\sum_P w_P(t, t_w)}, \tag{6}$$

where the weighting factor $w_P(t, t_w)$ is given by the intensity for the singly scattered waves arriving on the time window $(t - t_w, t + t_w)$.

3 SINGLE-SCATTERING MODEL

A seismic wave propagating in a spatially heterogeneous medium is treated as a source pulse that remains unaltered in wave shape despite interactions with the heterogeneities, plus scattered waves generated by the source pulse as it encounters heterogeneities in the medium. This is the basis of the single-scattering model.

In our numerical implementation of this single-scattering model we assume that the velocity field is a statistically homogeneous quasi-random medium, where small-scale velocity fluctuations with Gaussian autocorrelation function are added to a constant background velocity. The scale length of the velocity fluctuations is given by the correlation length a of the velocity fluctuations. The relative magnitude of the velocity fluctuations with respect to the mean is given by the standard deviation σ.

The single-scattering model assumes that the scattering is weak. For our random velocity model this implies that the magnitude of the velocity fluctuations σ is small so that the amplitude of the scattered waves is much smaller than the amplitude of the incident wave. Thus, as the incident wave propagates through the random medium, a small fraction of the energy of the incident is transformed into scattered energy due to the weak scattering.

By appropriately adjusting the values of a and σ for a given band-limited source signal, in Section 5 we calculate, using finite differences (second order in space, fourth order in space), synthetic seismograms such as the one shown in Fig. 1, which can be described using the single-scattering model. By this we mean that the energy loss of the incident wave by scattering is small. Also, the amplitude of the scattered waves is linearly proportional to the magnitude of the velocity fluctuations. For the sake of simplicity we ignore intrinsic attenuation and assume that the mass density is constant. If intrinsic attenuation is neglected, the dominant reduction in the amplitude of a propagating wave in this model is due to geometric spreading.

4 MEAN TRAVELTIME CHANGE IN THE SINGLE-SCATTERING REGIME

In the Born approximation the total wavefield u can be thought of as the summation of waves going over a multitude of paths, with all the possible paths defined by the single-scattering ellipses as shown in Fig. 1.

Each path from source to receiver is associated with a weight which is proportional to the intensity of the wave following that path. In the single-scattering regime this weight can be calculated using the Born approximation for the scattered intensity. Thus, recalling eq. (6), and considering the waves arriving within the time window $(t - t_w, t + t_w)$ we can calculate the average or mean traveltime change $\langle\tau\rangle(t)$ for the waves as the weighted average of the traveltime perturbations τ_P for waves that travel along different paths P.

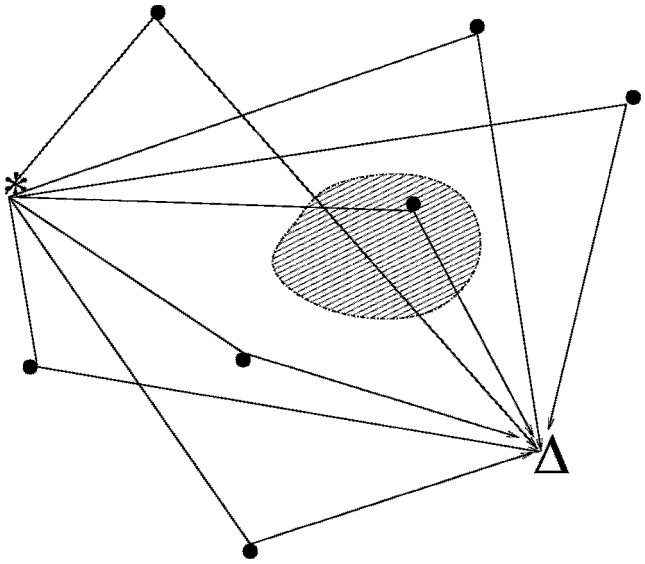

Figure 2. A wavefield generated at the source (asterisk) interacts with scattering heterogeneities and is recorded at the receiver (triangle).

Fig. 2 shows a cartoon representation of the paths that waves can follow in the single-scattering medium. The total wavefield is regarded as the superposition of many waves following different paths. Each wave starts at the source location, is scattered once with the heterogeneities, and finally, it is detected at the receiver location. If we introduce a localized perturbation in the propagation velocity (as shown by the shaded area in Fig. 2) some paths traverse the perturbation while others do not. This localized velocity change will perturb the traveltimes of the individual paths in a different way. The mean traveltime change $\langle\tau\rangle(t)$ averages out the different traveltime perturbations within a given time window.

4.1 Single-scattering intensity

Sato (1977) derived the space–time dependence of the energy density of scattered waves in 3-D assuming single isotropic scattering due to uniformly distributed scatterers. His model explains how scattered energy is homogeneously distributed as time increases. In this approach, the scattered field is assumed to be linearly proportional to the perturbations in the constitutive parameters (in our case, the acoustic velocity). In this study we use this approach to describe the time–space evolution of the intensity of the scattered waves.

First, we derive the expression for the time–space dependent intensity for an isotropic source in a statistically homogeneous random medium in the single-scattering regime. This gives the intensity $I_P(t)$ of a singly scattered wave with traveltime t and path P. The derivation is shown for scalar waves in two dimensions (2-D). Suppose that the propagation velocity $v(\mathbf{x})$ can be represented as a perturbation from a constant background velocity v_0 such that

$$v(\mathbf{x}) = v_0(1 + n(\mathbf{x})), \tag{7}$$

where $n(\mathbf{x})$ is a quasi-random perturbation added to the homogeneous background. For the present discussion, $n(\mathbf{x})$ is assumed to be small ($n(\mathbf{x}) \ll 1$) so that

$$\frac{1}{v^2(\mathbf{x})} = \frac{1}{{v_0}^2}(1 - 2n(\mathbf{x})). \tag{8}$$

In the last equation we have retained only the first-order term of an expansion about powers of $n(\mathbf{x})$, this is consistent with the Born approximation. The Helmholtz equation is given by

$$\nabla^2 u + \frac{\omega^2}{{v_0}^2}[1 - 2n(\mathbf{x})]u = 0. \tag{9}$$

The solution to the Helmholtz equation in the Born approximation is, in the frequency domain, given by (Bleistein *et al.* 2001)

$$u(\mathbf{x_g}, \mathbf{x_s}, \omega) = u_0(\mathbf{x_g}, \mathbf{x_s}, \omega) + 2\frac{\omega^2}{{v_0}^2}\int_A n(\mathbf{x})u_0(\mathbf{x}, \mathbf{x_s}, \omega) \times G_0(\mathbf{x_g}, \mathbf{x}, \omega)\, dA(\mathbf{x}), \tag{10}$$

where $u_0(\mathbf{x}_g, \mathbf{x}_s)$ is the incident or unperturbed wavefield generated at source location $\mathbf{x_s}$. The integration is over the locations $\mathbf{x}$ along the single-scattering ellipses. The term $G_0(\mathbf{x_g}, \mathbf{x})$ represents the free space Green's function that satisfies the Helmholtz equation for the homogeneous medium with velocity v_0:

$$\left[\nabla^2 + \frac{\omega^2}{{v_0}^2}\right] G_0(\mathbf{x_g}, \mathbf{x}, \omega) = \delta(\mathbf{x_g} - \mathbf{x}). \tag{11}$$

The free space Green's function in two dimensions $G_0(\mathbf{x_g}, \mathbf{x}, \omega)$ is

$$G_0(\mathbf{x_g}, \mathbf{x}, \omega) = -\frac{i}{4} H_0{}^{(1)}(k|\mathbf{x_g} - \mathbf{x}|), \tag{12}$$

where $H_0{}^{(1)}$ is the first Hankel function of degree zero and $k = \omega/v_0$ is the wavenumber. In the far field, the Hankel function is given by

$$H_0^{(1)}(k|\mathbf{x_g} - \mathbf{x}|) = \frac{e^{ik|\mathbf{x_g}-\mathbf{x}|-i\pi/4}}{\sqrt{\frac{\pi}{2}k|\mathbf{x_g} - \mathbf{x}|}}. \tag{13}$$

The scattered field u_s is given by the second term on the right hand side of eq. (10), that is,

$$u_s(\mathbf{x_g}, \mathbf{x_s}, \omega) = 2\frac{\omega^2}{v_0{}^2} \int_A G_0(\mathbf{x_g}, \mathbf{x}, \omega)\, n(\mathbf{x})\, u_0(\mathbf{x}, \mathbf{x_s}, \omega) \times dA(\mathbf{x}). \tag{14}$$

For a point source, the incident field $u_0(\mathbf{x}, \mathbf{x_s}, \omega)$ is equal to the impulse response or Green's function $G_0(\mathbf{x}, \mathbf{x_s}, \omega)$ and

$$u_s(\mathbf{x_g}, \mathbf{x_s}, \omega) = 2\frac{\omega^2}{v_0{}^2} \int_A G_0(\mathbf{x_g}, \mathbf{x}, \omega)\, n(\mathbf{x})\, G_0(\mathbf{x}, \mathbf{x_s}, \omega) \times dA(\mathbf{x}). \tag{15}$$

Substituting eqs (12) and (13) into eq. (14) and setting the distances $|\mathbf{x} - \mathbf{x_s}| = r_s$ and $|\mathbf{x_g} - \mathbf{x}| = r_g$ we get

$$\begin{aligned} u_s(\mathbf{x_g}, \mathbf{x_s}, \omega) &= -\frac{\omega^2}{4\pi v_0{}^2} \int_A \frac{e^{ik(r_s+r_g)-i\pi/2}\, n(\mathbf{x})}{k\sqrt{r_s r_g}}\, dA(\mathbf{x}) \\ &= \frac{(-i\omega)}{4\pi v_0} \int_A \frac{e^{ik(r_s+r_g)}\, n(\mathbf{x})}{\sqrt{r_s r_g}}\, dA(\mathbf{x}). \end{aligned} \tag{16}$$

To go to the time domain we multiply eq. (16) with $e^{-i\omega t}$ and integrate over angular frequencies ω:

$$u_s(\mathbf{x_g}, \mathbf{x_s}, t) = \frac{1}{4\pi v_0} \int_A dA(\mathbf{x}) \times \int_{-\infty}^{+\infty} (-i\omega) \frac{\exp\left[-i\omega\left(t - \frac{r_s + r_g}{v_0}\right)\right]}{\sqrt{r_s r_g}}\, n(\mathbf{x})\, d\omega. \tag{17}$$

Since $n(\mathbf{x})$, r_s and r_g do not depend on ω we can write

$$u_s(\mathbf{x_g}, \mathbf{x_s}, t) = \frac{1}{4\pi v_0} \int_A dA(\mathbf{x}) \frac{n(\mathbf{x})}{\sqrt{r_s r_g}} \times \int_{-\infty}^{+\infty} (-i\omega) \exp\left[-i\omega\left(t - \frac{r_s + r_g}{v_0}\right)\right] d\omega. \tag{18}$$

Using the differentiation and shifting property of Fourier transforms we obtain

$$u_s(\mathbf{x_g}, \mathbf{x_s}, t) = \frac{1}{2v_0} \int_A \frac{n(\mathbf{x})}{\sqrt{r_s r_g}} \frac{d}{dt}\left[\delta\left(t - \frac{(r_s + r_g)}{v_0}\right)\right] dA(\mathbf{x}). \tag{19}$$

Eq. (19) states that the total wavefield is the superposition of waves scattered with the heterogeneities defined by $n(\mathbf{x})$, with a geometric spreading decay given by the factor $\sqrt{r_s r_g}$ and with traveltime $t = (r_s + r_g)/v_0$. The time derivative of the delta function accounts for a $\pi/2$ phase change of the scattered waves. Now let us compute the average intensity from the scattered wavefield obtained in eq. (19). The intensity is given by

$$I(t) = u_s{}^2(t) + u^H{}_s{}^2(t), \tag{20}$$

where $u^H{}_s$ is the Hilbert transform of the scattered wavefield. Setting

$$S(t, \mathbf{x}) = \frac{d}{dt}\left[\delta\left(t - \frac{(r_s + r_g)}{v_0}\right)\right]. \tag{21}$$

We then have

$$u_s(\mathbf{x_g}, \mathbf{x_s}, t) = \frac{1}{2v_0} \int_A \frac{n(\mathbf{x})}{\sqrt{r_s r_g}}\, S(t, \mathbf{x})\, dA(\mathbf{x}). \tag{22}$$

Inserting eqs (19), (22) and its corresponding expression for its Hilbert transform into eq. (20) we obtain

$$\begin{aligned} I(\mathbf{x_s}, \mathbf{x_g}, t) = &\frac{1}{4v_0{}^2} \int_{A_1}\int_{A_2} dA_1(\mathbf{x_1}) dA_2(\mathbf{x_2}) \frac{n(\mathbf{x_1})}{\sqrt{r_{s_1} r_{g_1}}} \frac{n(\mathbf{x_2})}{\sqrt{r_{s_2} r_{g_2}}} \\ &\times \left[S(t, \mathbf{x_1}) S(t, \mathbf{x_2}) + S^H(t, \mathbf{x_1}) S^H(t, \mathbf{x_2})\right]. \end{aligned} \tag{23}$$

The mean intensity is obtained after calculating the ensemble average of the intensity, that is,

$$\begin{aligned} \langle I(\mathbf{x_s}, \mathbf{x_g}, t)\rangle = &\frac{1}{4v_0{}^2} \int_{A_1}\int_{A_2} dA_1(\mathbf{x_1}) dA_2(\mathbf{x_2}) \frac{\langle n(\mathbf{x_1})\, n(\mathbf{x_2})\rangle}{\sqrt{r_{s_1} r_{g_1}}\, \sqrt{r_{s_2} r_{g_2}}} \\ &\times \left[S(t, \mathbf{x_1}) S(t, \mathbf{x_2}) + S^H(t, \mathbf{x_1}) S^H(t, \mathbf{x_2})\right], \end{aligned} \tag{24}$$

where $\langle \ldots \rangle$ denotes ensemble averaging. When the correlation length a of the velocity fluctuations $n(\mathbf{x})$ is much smaller than the seismic wavelength, we can approximate

$$\langle n(\mathbf{x_1})\, n(\mathbf{x_2})\rangle = \langle n^2\rangle \delta(\mathbf{x_1} - \mathbf{x_2}). \tag{25}$$

Inserting this into eq. (24) we obtain

$$\langle I(\mathbf{x_s}, \mathbf{x_g}, t)\rangle = \frac{1}{4{v_0}^2} \int_A \frac{\langle n^2(\mathbf{x})\rangle}{r_s r_g}\, W\left(t - \frac{r_s + r_g}{v_0}\right) dA(\mathbf{x}), \tag{26}$$

where

$$W\left(t - \frac{r_s + r_g}{v_0}\right) = \left[S^2\left(t - \frac{r_s + r_g}{v_0}\right) + S^{H^2}\left(t - \frac{r_s + r_g}{v_0}\right)\right], \tag{27}$$

where $W(t - (r_s + r_g)/v_0)$ is the envelope of the source wavelet. In the high frequency approximation the envelope of the source function can be approximated as

$$W\left(t - \frac{r_s + r_g}{v_0}\right) \simeq \delta\left(t - \frac{r_s + r_g}{v_0}\right), \tag{28}$$

and the mean intensity becomes

$$\langle I(\mathbf{x_s}, \mathbf{x_g}, t)\rangle = C \int_A \frac{\langle n^2(\mathbf{x})\rangle}{r_s r_g}\, \delta\left(t - \frac{r_s + r_g}{v_0}\right) dA(\mathbf{x}), \tag{29}$$

where C is a constant. eq. (29) represents the total average intensity at receiver $\mathbf{x_s}$ due to an impulse generated at the source location $\mathbf{x_s}$ and transmitted through the scattering medium. Let us look just at the contribution to the total intensity of an area element $dA(\mathbf{x})$ at location $\mathbf{x}$. The contribution to the total intensity of the wavefield will be

$$\langle dI(\mathbf{x_s}, \mathbf{x_g}, t)\rangle = C \frac{\langle n^2(\mathbf{x})\rangle}{r_s r_g}\, \delta\left(t - \frac{r_s + r_g}{v_0}\right) dA(\mathbf{x}). \tag{30}$$

Eq. (30) is the contribution to the total intensity from an area element dA located at point $\mathbf{x}$. However, this can also be interpreted as the intensity of the singly scattered waves with paths P visiting location $\mathbf{x}$.

In eq. (6) the mean traveltime change is an average of the traveltime changes of every path P weighted by the intensity of the wave going along that path. It is easier though to consider the contribution of an area element $dA(\mathbf{x})$ to the total intensity and then integrate over the whole area. In this way we replace the discrete summation over paths by an integration over area elements, and $\langle dI(\mathbf{x_s}, \mathbf{x_g}, t)\rangle$ substitutes the weight factor or intensity of the paths $w_p(t, t_w)$ in eq. (6). All the possible paths P are included if we integrate over the area within the single-scattering ellipse. Since the constant C cancels out because it appears in both the numerator and the denominator, we define $w(\mathbf{x}, t)$ as the weight factor for the ensemble averaging over area

$$w(\mathbf{x}, t) = \frac{\langle n^2(\mathbf{x})\rangle}{r_s r_g}\, \delta\left(t - \frac{r_s + r_g}{v_0}\right). \tag{31}$$

Integrating over the whole area within the single-scattering ellipse has replaced summing over all the possible scattering paths P and in this way the calculation is greatly simplified.

4.2 Integral representation for the mean traveltime change in the single-scattering regime

We now turn our attention to the change that a wave with path P undergoes when we introduce a small change in the propagation velocity. Suppose that the background slowness in a certain region is perturbed by an amount $\delta\mathbf{s}(\mathbf{x})$ small enough that the ray is essentially unchanged (see Fig. 3). The traveltime of the scattered wave with trajectory P is given by

$$t_P = \int_{l_s} \frac{1}{v_0}\, dl + \int_{l_g} \frac{1}{v_0}\, dl = \frac{r_s + r_g}{v_0}, \tag{32}$$

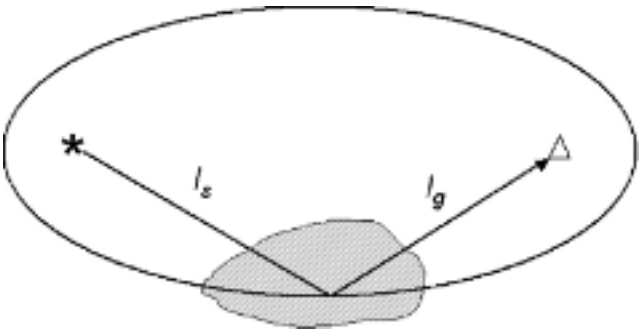

Figure 3. Geometry of a single-scattering path P: l_s is the path from the source (asterisk) to the edge of the ellipse and l_g is the path from the edge of the ellipse to the receiver (triangle). The shaded area indicates a perturbation in the slowness.

where l_s represents the straight path from the source at $\mathbf{x_s}$ to a given scatterer on the ellipse, and l_g represents the straight path from the scatterer to the receiver location $\mathbf{x_g}$; r_s and r_g are the lengths of the paths l_s and l_g respectively.

Expressing the traveltime t_P in terms of the mean slowness $\mathbf{s}_0$, this integral is given by

$$t_P = \int_{l_s} \mathbf{s}_0 \, dl + \int_{l_g} \mathbf{s}_0 \, dl = \frac{r_s + r_g}{v_0}. \tag{33}$$

We introduce a small perturbation in the slowness $\delta\mathbf{s}_0(\mathbf{x})$ such that the perturbed slowness is $\mathbf{s}_p(\mathbf{x}) = \mathbf{s}_0 + \delta\mathbf{s}(\mathbf{x})$. After the perturbation, the traveltime of the path P changes by

$$\tau_P \simeq \int_P \delta\mathbf{s}(\mathbf{x}) \, dl(\mathbf{x}) = \int_{l_s} \delta\mathbf{s}(\mathbf{x}) \, dl(\mathbf{x}) + \int_{l_g} \delta\mathbf{s}(\mathbf{x}) \, dl(\mathbf{x}), \tag{34}$$

where l_s and l_g are the ray paths through the reference medium. The assumption here is that the slowness perturbation is small (compared to the reference or mean slowness) such that we can linearize the expression in eq. (33) with respect to the slowness. The traveltime change τ_P represents the propagation time change of the wave that propagates through the medium with trajectory P and time t_P. The approximation in eq. (34) is the application of Fermat's theorem to traveltime tomography (Aldridge 1994).

We can use the changes in the traveltime τ_P to study the localized slowness change in the medium. In eq. (6) the mean traveltime change $\langle\tau\rangle(t)$ was expressed as the sum over the paths P dictated by the single-scattering ellipsoids. As described in the previous section, it is more convenient to replace the sum over paths with an integration over area. The mean traveltime change can thus be rewritten as

$$\langle\tau\rangle(t) = \frac{\int_A \tau(\mathbf{x}) \, w(\mathbf{x}, t) \, dA(\mathbf{x})}{\int_A w(\mathbf{x}, t) \, dA(\mathbf{x})}, \tag{35}$$

where the traveltime change $\tau(\mathbf{x})$ corresponds to the traveltime change of the two paths $P1$ and $P2$ going through $\mathbf{x}$ as depicted in Fig. 4. The weight $w(\mathbf{x}, t)$ corresponds to the intensity of the paths P with traveltime t going through $\mathbf{x}$. The integration is over the area where scattering takes place so that all possible paths P are included in the integral defined in eq. (35). Inserting eqs (31) and (34) into eq. (35) we obtain

$$\langle\tau\rangle(t) = \frac{\int_A \left[\int_{l_s(\mathbf{x})} \delta\mathbf{s}(\mathbf{x}) \, dl(\mathbf{x}) + \int_{l_g(\mathbf{x})} \delta\mathbf{s}(\mathbf{x}) \, dl(\mathbf{x})\right] \times \frac{n^2(\mathbf{x})}{r_s r_g} \, \delta\left(t - \frac{r_s + r_g}{v_0}\right) \, dA(\mathbf{x})}{\int_A \frac{n^2(\mathbf{x})}{r_s r_g} \, \delta\left(t - \frac{r_s + r_g}{v_0}\right) \, dA(\mathbf{x})}. \tag{36}$$

The area of integration is delimited by the single-scattering ellipse at traveltime t for source and receiver located at $\mathbf{x_s}$ and $\mathbf{x_g}$, respectively. In Appendix A we solve the integrals using elliptical coordinates and obtain the following expression for the mean traveltime change of scattered waves in the single-scattering regime

$$\langle\tau\rangle(t) = \frac{1}{2\pi h \sqrt{\left(\frac{v_0 t}{2h}\right)^2 - 1}} \int_A \left[\frac{r_s}{s} + \frac{r_g}{g}\right] \delta\mathbf{s}(\mathbf{x}) \, dA(\mathbf{x}), \tag{37}$$

where h is the half-distance between source and receiver and we have made use of the geometrical variables specified in Fig. 5. Note that this result is independent of $n(\mathbf{x})$, which is a measure of the scattering strength of the medium. Eq. (37) accounts for the average change in the traveltime of singly scattered waves due to a localized slowness perturbation $\delta\mathbf{s}(\mathbf{x})$. This expression gives the linearized relationship between the mean traveltime change and the localized slowness perturbation $\delta\mathbf{s}(\mathbf{x})$, that is,

$$\langle\tau\rangle(t) = \int_A K(\mathbf{x}, t) \, \delta\mathbf{s}(\mathbf{x}) \, dA(\mathbf{x}), \tag{38}$$

where $K(\mathbf{x}, t)$ is the integration kernel that relates the mean traveltime change at traveltime t with a localized slowness perturbation at $\mathbf{x}$ for a given source and receiver configuration, and is given by

$$K(\mathbf{x}, t) = \frac{1}{2\pi h \sqrt{\left(\frac{v_0 t}{2h}\right)^2 - 1}} \left[\frac{r_s}{s} + \frac{r_g}{g}\right]. \tag{39}$$

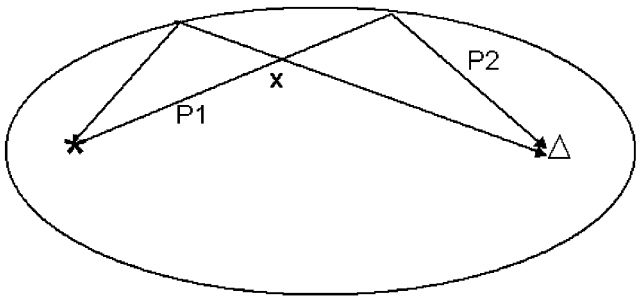

Figure 4. Single-scattering paths that intersect location $\mathbf{x}$.

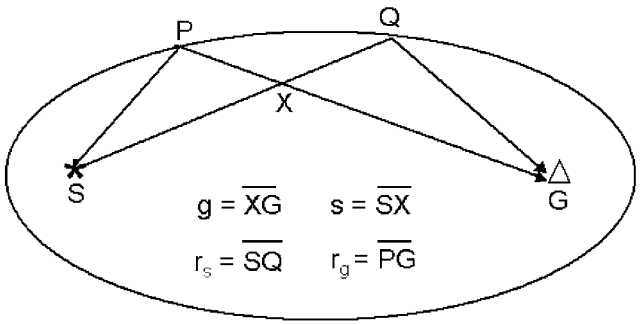

Figure 5. Geometry used in the derivation of eq. (37).

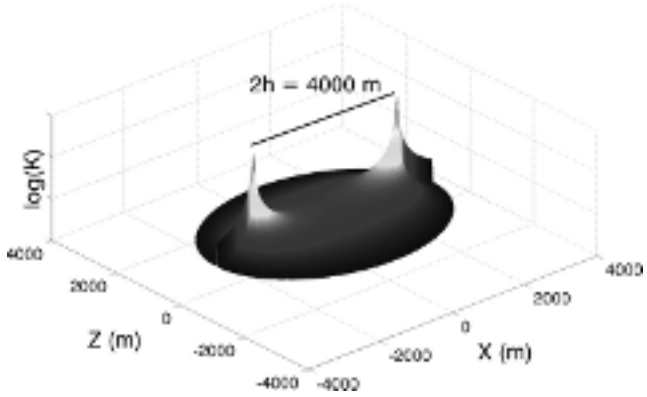

Figure 6. Logarithm of K as function of location for $h = 2000$ m and $t = 1$ s. The background velocity v_0 is 6000 m s^{-1}.

The kernel $K(\mathbf{x}, t)$ is the sensitivity function of the mean traveltime change for the localized slowness perturbation. It has dimensions of 1/distance. Fig. 6 shows the logarithm of K as a function of location for half source–receiver distance $h = 2000$ m and propagation time $t = 1$ *s*. The distribution is peaked at the source and receiver locations, and decreases rapidly from both locations until it vanishes outside the single-scattering ellipse described by the traveltime t. In the next section we use eq. (37) to calculate numerically the mean traveltime change for a localized perturbation for different source and receiver geometries.

5 TRAVELTIME CHANGE FROM FINITE-DIFFERENCE SYNTHETICS

We validate our theory with synthetic seismograms of acoustic waves calculated with a fourth-order finite-difference algorithm before and after a localized slowness perturbation has been introduced in the medium. As described in Section 3 the velocity model is characterized as a constant background velocity with added small random velocity fluctuations. The correlation distance a is 40 m, which is small compared to the dominant wavelength of 240 m for the Gaussian shaped source wavelet employed. We set the value for σ (relative magnitude of the velocity fluctuations with respect to the background velocity $v_0 = 6000$ m) such that the scattering is weak and the single-scattering approximation is valid. For the example shown here we use $\sigma = 2$ per cent.

We perturb the initial velocity model by adding a localized constant slowness perturbation to it. This slowness perturbation is small and smooth. Fig. 7 shows the localized perturbation of the mean slowness in the shape of a square with sides of length equal to 3000 m. The magnitude of the slowness perturbation with respect to the mean slowness is $\delta\mathbf{s}/\mathbf{s}_0 = 0.005$. We calculate the synthetic seismograms for the unperturbed and perturbed velocity model. Fig. 8 shows, as an example, both the unperturbed and perturbed seismograms for receiver **R2** located 5500 m away from the source. At first sight there seems to be no substantial difference between the wavefields before and after the perturbation but looking more closely (see Fig. 9), we can clearly see that one seismogram lags with respect to the other. More careful inspection indicates that the behaviour of the time lags as a function of traveltime is systematic. It is this variation in the traveltime change as a function of propagation time t the one that we seek to predict with our theory.

We calculate the theoretical mean traveltime change for the single-scattering wavefield recorded at the receivers pictured in Fig. 7 and compare the result with the mean traveltime change estimated from the synthetic seismograms using the time-windowed cross-correlation as described by Snieder *et al.* (2002). The comparison is shown in Figs 10, 11, 12 and 13. The theoretical mean traveltime change $\langle\tau\rangle(t)$ was calculated using eq. (37) for a range of traveltimes t. The mean traveltime of the synthetic seismograms was obtained using the time-windowed cross-correlation technique using a window length of 500 ms (approximately 12 periods at the dominant frequency).

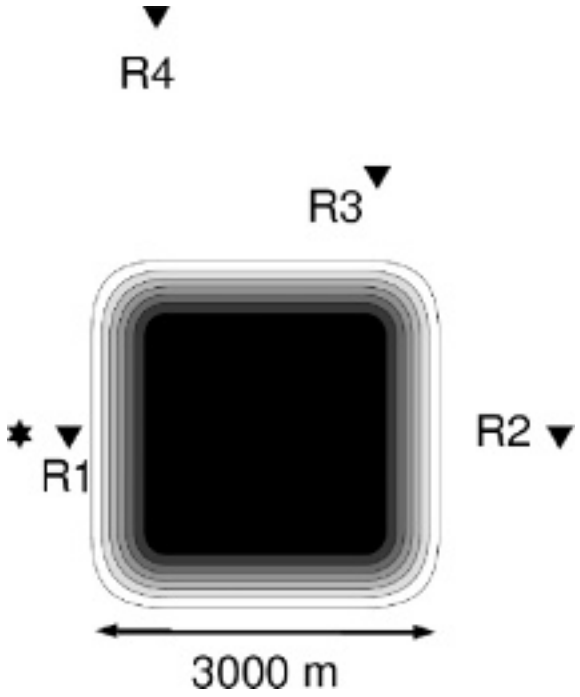

Figure 7. Perturbation of the slowness added to the initial velocity model to create the perturbed velocity model. The side length of the square is 3000 m and the magnitude of the perturbation is $\delta s_0/s_0 = 0.0050$. Source is shown as a star and the four receivers are shown as triangles.

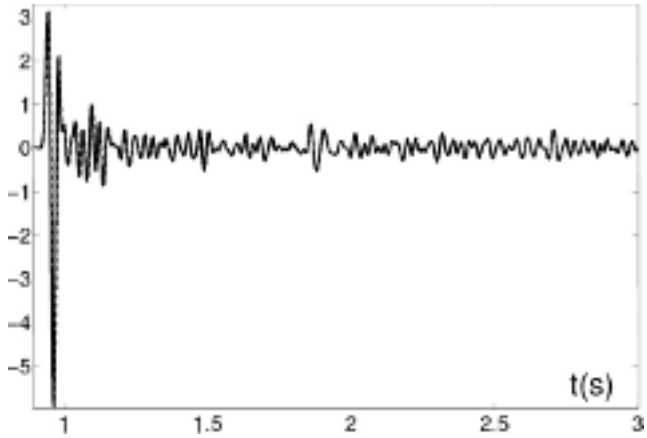

Figure 8. Unperturbed (solid) and perturbed (dashed) synthetic seismograms for receiver **R2** located 5500 m away from the source.

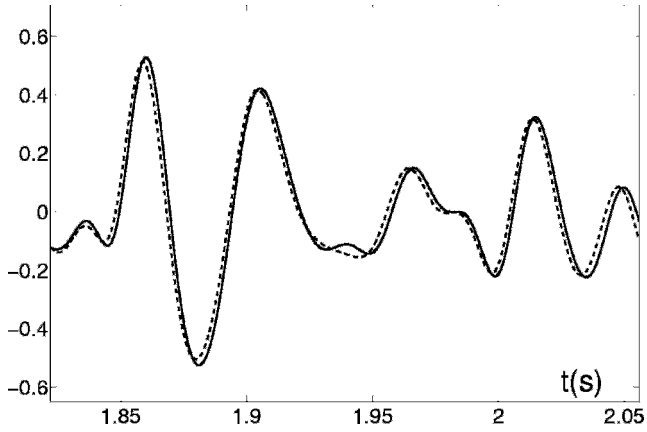

Figure 9. Closer view to the unperturbed (solid) and perturbed (dashed) synthetic seismograms for receiver **R2** located 5500 m away from the source.

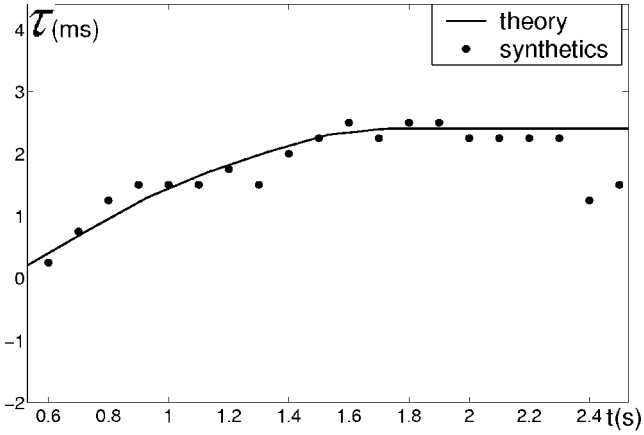

Figure 10. Theoretical versus measured mean traveltime change for receiver **R1** located 500 m from the source. The window length in the cross-correlation is 500 ms.

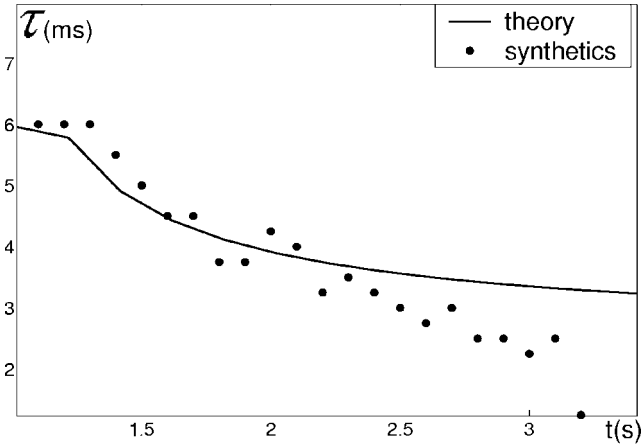

Figure 11. Theoretical versus measured mean traveltime change for receiver **R2** located 5500 m away from the source. The window length in the cross-correlation is 500 ms.

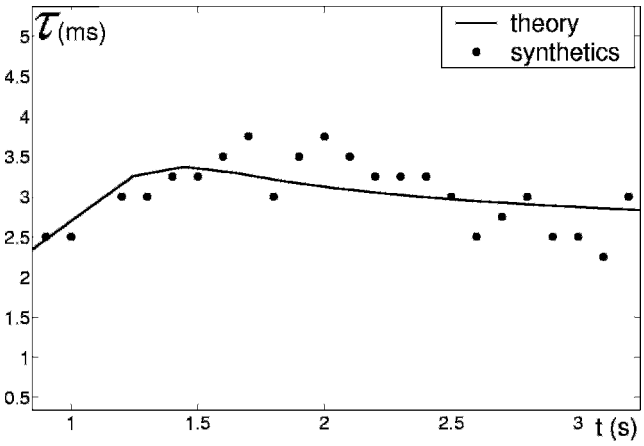

Figure 12. Theoretical versus measured mean traveltime change for receiver **R3** located 4500 m away from the source. The window length in the cross-correlation is 500 ms.

Fig. 10 shows the mean traveltime change for receiver **R1** located 500 m away from the source and ahead of the localized slowness perturbation. Notice that the mean traveltime change starts increasing and then reaches a maximum. For receiver **R2** the mean traveltime change decreases from a maximum at $t = 1.0$s. We also show the mean traveltime change for receivers **R3** and **R4** in Figs 12 and 13, respectively. Despite fluctuations about the predicted mean traveltime change (because of the randomness of the model), there is a good agreement between the theoretical and the measured mean traveltime change $\langle\tau\rangle(t)$ for all cases shown here.

For different source–receiver pairs we obtain different values of the mean traveltime change as a function of time. This difference can be better understood if we look at the single-scattering ellipses that define the paths for different receivers. In Fig. 14 we show the single-scattering

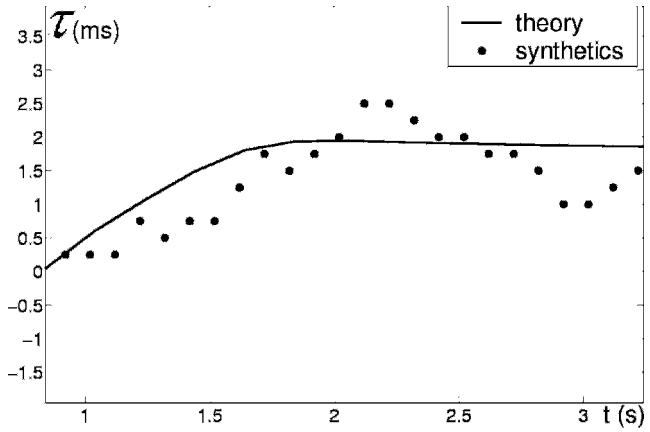

Figure 13. Theoretical versus measured mean traveltime change for receiver **R4** located 4500 m away from the source. The window length in the cross-correlation is 500 ms.

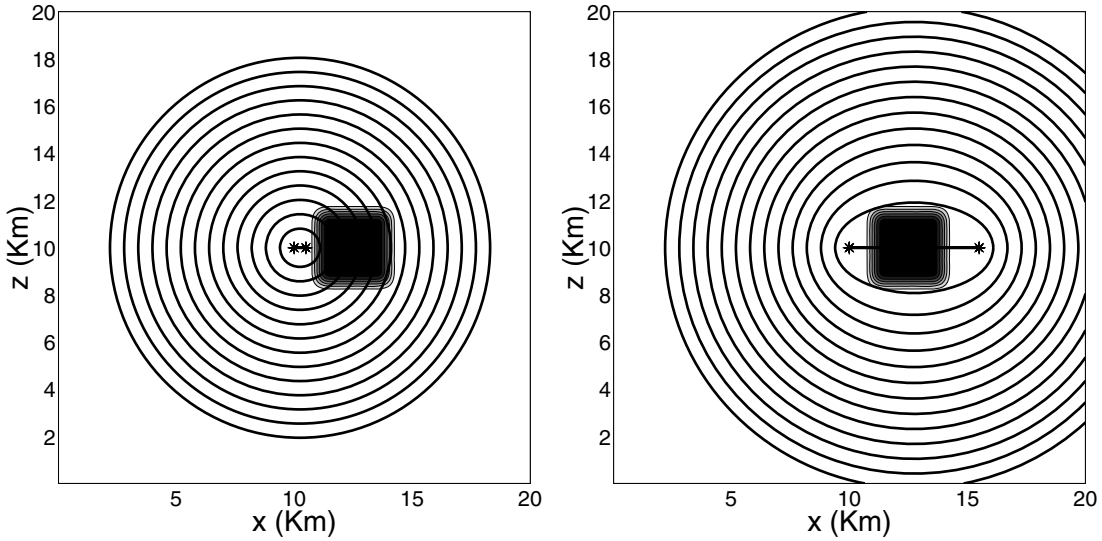

Figure 14. Single-scattering ellipses for receiver **R1** (left panel) and receiver **R2**. Source and receiver locations are indicated by asterisks.

ellipses for receivers **R1** (left panel) and receiver **R2** (right panel). For receiver **R1** and for early propagation times, the paths do not sample the slowness perturbation. As the propagation time increases the ellipses broaden and sample a larger piece of the perturbation. For receiver **R2** on the other hand, for early times, the perturbation occupies relatively a larger portion of the ellipses and, therefore, more paths are affected by the perturbation. For larger traveltimes the ellipses occupy relatively smaller portions of the ellipses and in this case a larger fraction of the paths go around the perturbation, decreasing the mean traveltime change. The difference in the traveltime change for different source and receiver pairs can be exploited in a tomographic scheme to invert the mean traveltime change information to estimate the location and magnitude of the slowness perturbation in a linearized inverse problem formulation based on eq. (38).

We compare the mean traveltime change calculated for the single-scattering regime with the mean traveltime change calculated for the multiple scattering regime for the same slowness perturbation using the technique developed by Pacheco & Snieder (2005). The value of $n(\mathbf{x})$ is larger in the multiple scattering example in order to generate stronger scattering events. Fig. 15 shows such a comparison for receiver **R2**. Notice the different behaviour of the theoretical mean traveltime change for the single and for the multiple scattering case. At $t = 1$s both approximations give the same mean traveltime change (the traveltime change of the direct arrival in the single-scattering case, and the traveltime change of the coherent wave for the multiple scattering case) but for later traveltimes the mean traveltime change for multiply scattered waves increases as a function of time, while the mean traveltime change for singly scattered waves decreases as a function of time. This difference is due to the fact that the multiply scattered waves sample a given area more often than the singly scattered waves do.

6 DISCUSSION AND CONCLUSIONS

In the synthetic examples of the previous section we observed fluctuations of the measured mean traveltime change from the calculated finite-difference seismograms around the theoretical value calculated using eq. (37). The fluctuations are due to the random nature of the scattered wavefield.

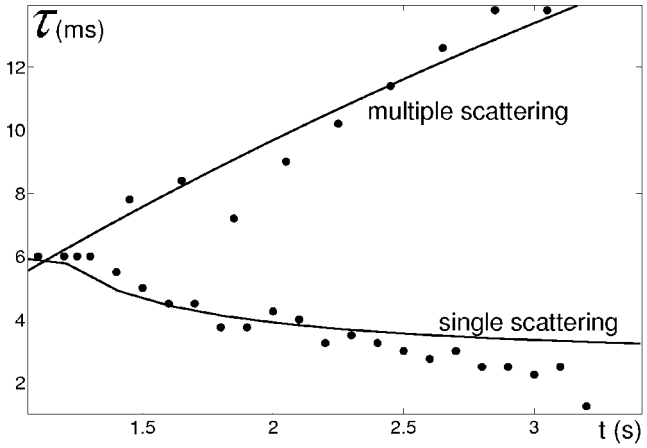

Figure 15. Comparison between mean traveltime change for single and for multiple scattering for receiver **R2** for the same slowness perturbation, that is, same $\delta s(\mathbf{x})$. The window length in the cross-correlation is 500 ms (approximately 12 periods).

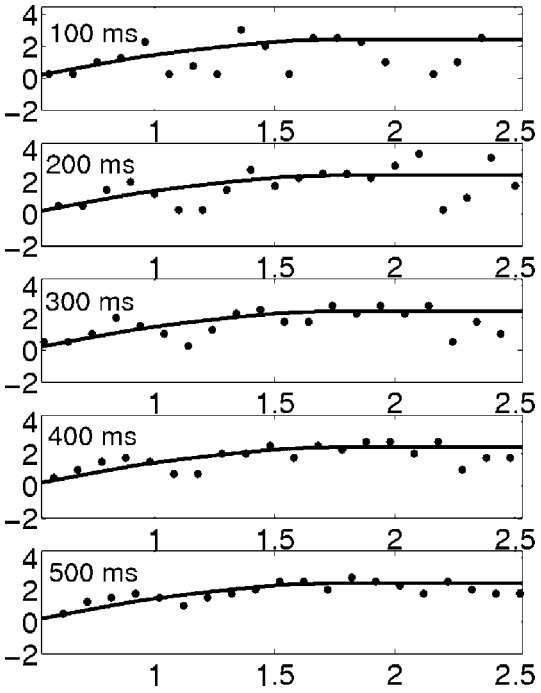

Figure 16. Comparison between the $\langle\tau\rangle(t)$ of the synthetic seismograms (dots) versus the theoretical $\langle\tau\rangle(t)$ for different lengths of the time window (indicated on the upper left corner of each plot) used in the cross-correlation of the unperturbed and perturbed seismograms for receiver **R1**. The theoretical mean traveltime change is shown as the solid line.

The fluctuations in the mean traveltime change estimated from the synthetic seismograms are due to the fact that we have only a single realization of the scattered wavefield. We measure the mean traveltime change from the synthetic seismograms using a time-windowed cross-correlation technique. The mean traveltime change measured in this way is a weighted average of the time lag for the many scattered waves that arrive within that time window. The time averaging we use in the time-windowed cross-correlation reduces the fluctuations of the measured mean traveltime change. Snieder (2004) shows that we can reduce these fluctuations by a factor $1/\sqrt{\Delta f t_w}$, where Δf is the bandwidth of the data, and $2t_w$ as the length of the time window.

The decrease in the fluctuations with the increase of the time-window length $2t_w$ is shown in Fig. 16 where we plot the measured $\langle\tau\rangle(t)$ versus propagation time t using different window lengths for the time-windowed cross-correlation for the receiver **R1**. For this synthetic data example the dominant period is 40 ms. The length of the time window $2t_w$ varies from 100 to 500 ms. We see that the fluctuations of the measured $\langle\tau\rangle(t)$ indeed decrease with an increase of t_w.

In developing the expression of the mean traveltime change $\langle\tau\rangle(t)$ as an average over different paths we assume that the paths before and after the perturbation are the same. Should this not be the case, the weight of each scattering path looses significance. This imposes a constraint on the magnitude of the slowness perturbations that we can solve using our approximation, since the perturbations have to be small enough in order that the paths are preserved after the perturbation.

The most important result of this work is that we are able to predict the traveltime change of singly scattered waves in a statistical way without any knowledge of the scattering properties of the medium (no diffusion constant, mean free path or standard deviation of the velocity fluctuations σ value is required for the calculation). As long as we can describe the wavefield by means of the single-scattering approximation, the perturbation of the traveltime of the scattered waves depends linearly on the localized slowness perturbation. This technique has the potential of imaging time-lapse changes of the scattering medium. This technique can be used to detect temporal variations in the slowness of the medium for a random medium characterized by homogeneously distributed weak scatterers.

REFERENCES

Aki, K. & Chouet, B., 1975. Origin of coda waves: source, attenuation and scattering effects, *J. geophys. Res.,* **80**(23), 3322–3341.

Aldridge, D., 1994. Linearization of the eikonal equation, *Geophysics,* **59**(10), 1631–1632.

Bleistein, N., Cohen, J. & Stockwell, J., 2001. *Mathematics of Multidimensional Seismic Imaging, Migration and Inversion*, Vol. 13 of Interdisciplinary Applied Mathematics, Springer.

Chernov, L., 1960. *Wave Propagation in a Random Medium*, McGraw-Hill, New York.

Claerbout, J., 1985. *Imaging the Earth's Interior*, Blackwell.

Jian, Z., Pearce, J. & Mittleman, D., 2003. Characterizing individual scattering events by measuring the amplitude and phase of the electric field diffusing through a random medium, *Phys. Rev. Lett.,* **93**(3), 339 031–339 034.

Kopnichev, Y., 1977. The role of multiple scattering in the formation of a seismogram's tail, *Inveztiya Academy of Science USSR, Physics of the Solid Earth,* **13,** 394–398.

Leary, P.C., 2002. Numerical simulation of first-order backscattered p and s waves for time-lapse seismic imaging in heterogeneous reservoirs, *Geophys. J. Int.,* **148,** 402–425.

Morse, P. & Feshbach, H., 1953. *Methods of Theoretical Physics*, McGraw-Hill Book company, Inc.

Pacheco, C. & Snieder, R., 2005. Time-lapse traveltime change of multiply-scattered acoustic waves, *JASA,* **118**(3), 1300–1310.

Page, J., Schriemer, H., Bailey, A. & Weitz, D., 1995. Experimental test of the diffusion approximation for multiply scattered waves, *Phys Rev E,* **52**(3), 3106–3114.

Sato, H., 1977. Energy propagation icluding scattering effect: single isotropic scattering approximation., *J. Phys. Earth,* **25,** 27–41.

Schriemer, H., Cowan, M., Page, J., Liu, Z. & Weitz, D., 1997. Energy velocity of diffusing waves in strongly scattering media, *Phys Rev Lettters,* **79**(17), 3166–319.

Snieder, R., 1999. Imaging and averaging in complex media, in *Diffuse Waves in Complex Media*, pp. 405–454, ed. Fouque, J., Kluwer Academic Publishers.

Snieder, R., 2004. Extracting the Green's function from the correlation of coda waves: a derivation based on stationary phase, *Phys. Rev. E,* **69,** 046610.

Snieder, R., 2006. The theory of coda wave interferometry, *Pure Appl. Geophys.,* in press.

Snieder, R., Gret, A. & Douma, H., 2002. Coda wave interferometry for estimating nonlinear behavoir in seismic velocity, *Science,* **295**(22), 2253–2255.

Turner, J. & Weaver, R., 1994. Radiative transfer of ultrasound, *J. acoust. Soc. Am.,* **96,** 3654–3673.

Weitz, D. & Pine, D., 1993. Diffusing wave spectroscopy, in *Dynamic light scattering, The method and some applications*, pp. 652–720, ed. Brown, W., Clarendon Press, Oxford.

Wu, R., 1982. Attenuation of short period seismic waves due to scattering, *Geophys. Res. Lett.,* **9**(1), 9–12.

Yodh, A. & Chance, B., 1995. Spectroscopy and imaging with diffusing light, *Physics Today,* **48,** 34–40.

APPENDIX A: MEAN TRAVELTIME CHANGE FOR NON-COINCIDENT SOURCE AND RECEIVER

In this section we show the derivation of eq. (37) from eq. (36). Let us start with eq. (33), where $\delta s(\mathbf{x})$ is the localized slowness perturbation. The path l_s runs form the source to the edge of the ellipse, and the path l_g goes from the edge of the ellipse to the receiver. The term $\langle n^2(\mathbf{x})\rangle$ is approximately constant so we can take it out of the integrals in the numerator and denominator. If we replace $\delta(t - \frac{(r_s+r_g)}{v_0})$ with $v_0\delta\,(v_0 t - (r_s + r_g))$ we obtain

$$\langle\tau\rangle(t) = \frac{\int_A \left[\int_{l_s(\mathbf{x})} \delta\mathbf{s}(\mathbf{x})\, dl(\mathbf{x}) + \int_{l_g(\mathbf{x})} \delta\mathbf{s}(\mathbf{x}))\, dl(\mathbf{x})\right] \frac{1}{r_s r_g}\, \delta(v_0 t - (r_s + r_g))\, dA(\mathbf{x})}{\int_A \frac{1}{r_s r_g}\, \delta(v_0 t - (r_s + r_g))\, dA(\mathbf{x})}. \tag{A1}$$

This expression is complicated due to presence of the delta function inside the integrals. We use elliptical coordinates (Morse & Feshbach 1953) to evaluate the integration of the delta function. The elliptical coordinates θ and ε are defined by

$$\varepsilon = \frac{r_s + r_g}{2h}, \quad \cos(\theta) = \frac{r_s - r_g}{2h}, \quad x = h\varepsilon\cos(\theta), \quad y = h\sqrt{\varepsilon^2 - 1}\,\sin(\theta), \tag{A2}$$

where h is the half-distance from source to receiver, a is the half-length of the major axis of the ellipse, and θ is the angle formed between the line connecting the origin with location $\mathbf{x}$ (see Fig. A1). The delta function is in this coordinate system given by

$$\delta(v_0 t - (r_s + r_g)) = \delta(v_0 t - 2h\varepsilon) = \frac{1}{2h}\delta\left(\varepsilon - \frac{v_o t}{2h}\right). \tag{A3}$$

The element of area dA in elliptical coordinates is given by $dA = [\partial(x, y)/\partial(\varepsilon, \theta)]\, d\varepsilon\, d\theta$, where $[\partial(x, y)/\partial(\varepsilon, \theta)]$ is the Jacobian of the coordinate transformation, that is,

$$\frac{\partial(x, y)}{\partial(\varepsilon, \theta)} = \begin{vmatrix} \frac{\partial x}{\partial \varepsilon} & \frac{\partial y}{\partial \varepsilon} \\ \\ \frac{\partial x}{\partial \theta} & \frac{\partial y}{\partial \theta} \end{vmatrix} = \frac{h^2(\varepsilon^2 - \cos^2(\theta))}{\sqrt{\varepsilon^2 - 1}}. \tag{A4}$$

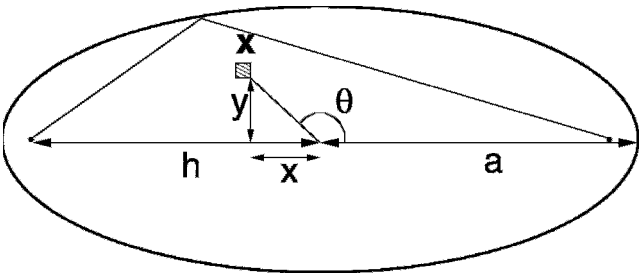

Figure A1. Geometry of the ellipse with centre at the origin.

Therefore, the area element becomes

$$dA = dx\,dy = \frac{h^2(\varepsilon^2 - \cos^2(\theta))}{\sqrt{\varepsilon^2 - 1}}\,d\varepsilon\,d\theta. \tag{A5}$$

In the integrals in eq. (A1) we need the combination $dA/r_s r_g$. Using the elliptical coordinates in eq. (A2) we find

$$r_s r_g = h(\varepsilon - \cos(\theta))h(\varepsilon + \cos(\theta)) = h^2(\varepsilon^2 - \cos^2(\theta)). \tag{A6}$$

We first solve for the denominator I_D in eq. (A1). Inserting eqs (A3), (A5) and (A6) into eq. (A1) we can write the denominator as

$$I_D = \int_A \frac{1}{r_s r_g}\delta(v_0 t - (r_s + r_g))\,dA(\mathbf{x}) = \int_0^{2\pi} d\theta \int_1^{\infty} d\varepsilon \frac{1}{2h\sqrt{\varepsilon^2 - 1}}\delta\left(\varepsilon - \frac{v_0 t}{2h}\right). \tag{A7}$$

Since the integrand does not depend on θ we obtain

$$I_D = \frac{\pi}{h}\int_1^{\infty} d\varepsilon \frac{1}{\sqrt{\varepsilon^2 - 1}}\delta\left(\varepsilon - \frac{v_0 t}{2h}\right). \tag{A8}$$

Using the shifting property of the delta function, and since $\varepsilon = v_0 t/2h$ lies within the interval of integration, we obtain

$$I_D = \frac{\pi}{h}\frac{1}{\sqrt{\left(\frac{v_o t}{2h}\right)^2 - 1}}, \tag{A9}$$

and we can write eq. (A1) as follows

$$\langle\tau\rangle(t) = \frac{1}{I_D}\int_0^{2\pi} d\theta \int_1^{+\infty} \frac{d\varepsilon}{\sqrt{\varepsilon^2 - 1}}\left[\int_{l_s(\mathbf{x})} \frac{1}{2h}\delta\left(\varepsilon - \frac{v_0 t}{2h}\right)\,\delta\mathbf{s}(\mathbf{x})\,dl(\mathbf{x}) + \int_{l_g(\mathbf{x})} \frac{1}{2h}\delta\left(\varepsilon - \frac{v_0 t}{2h}\right)\,\delta\mathbf{s}(\mathbf{x})\,dl(\mathbf{x})\right]. \tag{A10}$$

For convenience, we can write the expression of the mean traveltime change as the sum of the mean traveltime change from the source location $\mathbf{x_s}$ to the edge of the ellipse plus the mean traveltime change from the edge of the ellipse to the receiver location $\mathbf{x_g}$. Thus,

$$\langle\tau\rangle(t) = I_s + I_g, \tag{A11}$$

where I_s and I_g are

$$I_s = \frac{1}{I_D}\int_0^{2\pi} d\theta \int_1^{+\infty} \frac{d\varepsilon}{\sqrt{\varepsilon^2 - 1}}\int_{l_s(\mathbf{x})} \frac{1}{2h}\delta\left(\varepsilon - \frac{v_0 t}{2h}\right)\,\delta\mathbf{s}(\mathbf{x})\,dl(\mathbf{x}), \tag{A12}$$

$$I_g = \frac{1}{I_D}\int_0^{2\pi} d\theta \int_1^{+\infty} \frac{d\varepsilon}{\sqrt{\varepsilon^2 - 1}}\int_{l_g(\mathbf{x})} \frac{1}{2h}\delta\left(\varepsilon - \frac{v_0 t}{2h}\right)\,\delta\mathbf{s}(\mathbf{x})\,dl(\mathbf{x}). \tag{A13}$$

Let us first analyse the contribution to the mean traveltime change of the paths that start at the source and finish at the edge of the ellipse. Substituting the value of I_D from eq. (A12) and using again the shifting property of the delta function, we obtain

$$I_s = \frac{1}{2\pi}\int_0^{2\pi} d\theta \int_{l_s(\mathbf{x})} \delta\mathbf{s}(\mathbf{x})\,dl(\mathbf{x}). \tag{A14}$$

Eq. (A14) states that the mean traveltime change of paths starting at the source and ending at the edge of the ellipse is an average of the traveltime change of the different paths l_s for each value of θ. This looks simple enough, but it is not yet useful, as we would like the expression for the mean traveltime change to take the form of an area integral over the Cartesian coordinates x and y. The key is to realize that the combination of the θ-integral and the dl-integral sweeps over the whole interior of the single-scattering ellipse. Thus, we want to obtain the value of $d\theta dl$ as a function of $dxdy$. The question is, then, what is the scaling factor if rewrite eq. (A14) as an integral over the Cartesian coordinates x and y.

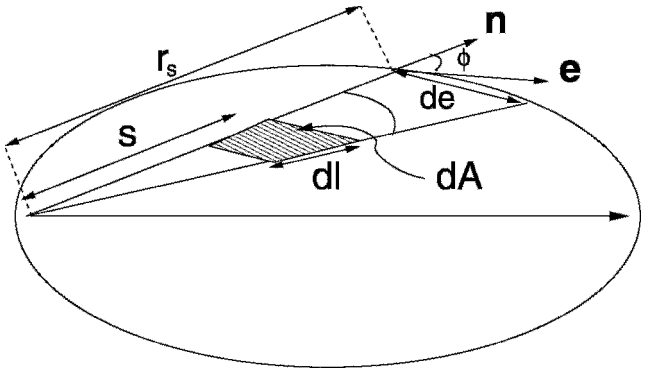

Figure A2. Relation between the area element dA and the length element dl for a path l_s starting at the source and ending at the edge of the ellipse. **n** is a unit vector that points on the direction of the path and **e** is a unit vector that points along the edge of the ellipse at the point of intersection of the path with the edge of the ellipse.

Let dl be an increment in length along the path l_s from the source location to the edge of the ellipse and de be an increment in length along the edge of the ellipse for an increment in angle $d\theta$. Then,

$$dA = \frac{s}{r_s}(\mathbf{dl} \times \mathbf{de}) = \frac{s}{r_s} dl\, de \sin(\phi), \tag{A15}$$

where ϕ is the angle between the unit vector **n** pointing along the direction of the path l_s and the vector **e** parallel to the edge of the ellipse on the point of intersection, as described in Fig. A2. The term s/r_s corrects for the fact that the surface area shrinks as we approach the source.

Let us compute the length element de along the edge of the ellipse. We get this by differentiating x and y in elliptical coordinates with respect to angle θ, that is,

$$de = \sqrt{dx^2 + dy^2}, \tag{A16}$$

where

$$dx = -h\, \varepsilon \sin(\theta)\, d\theta, \tag{A17}$$

and

$$dy = h\, \sqrt{\varepsilon^2 - 1}\, \cos(\theta)\, d\theta. \tag{A18}$$

Inserting eqs (A17) and (A18) into eq. (A16) we obtain

$$de = h\, \sqrt{\varepsilon^2 - \cos^2(\theta)}\, d\theta = h \sqrt{\left(\frac{v_o t}{2h}\right)^2 - \cos^2(\theta)}\, d\theta, \tag{A19}$$

where we have made the substitution $\varepsilon = v_0 t/2h$. In order to compute $\sin(\phi)$ we first construct the unit vectors **n** and **e**, and then, calculate the magnitude of the cross-product of the two vectors. The vector **n** points away from the source along the path l_s. The vector **e** points along the edge of the ellipse. According to the geometry specified in Fig. A3 we have

$$\mathbf{n} = \frac{1}{\sqrt{(x+h)^2 + y^2}} \begin{pmatrix} x+h \\ y \end{pmatrix} = \frac{1}{\sqrt{(h\cos(\theta) + h)^2 + (h\sqrt{\varepsilon^2 - 1}\, \sin(\theta))^2}} \begin{pmatrix} h\cos(\theta) + h \\ h\sqrt{\varepsilon^2 - 1}\, \sin(\theta) \end{pmatrix}. \tag{A20}$$

After some algebra we obtain

$$\mathbf{n} = \frac{1}{\varepsilon + \cos(\theta)} \begin{pmatrix} \varepsilon\cos(\theta) + 1 \\ \sqrt{\varepsilon^2 - 1}\, \sin(\theta) \end{pmatrix}. \tag{A21}$$

The vector **e** points along the edge of the ellipse and is given by

$$\mathbf{e} = \frac{1}{\sqrt{\left(\frac{\partial x}{\partial \theta}\right)^2 + \left(\frac{\partial y}{\partial \theta}\right)^2}} \begin{pmatrix} \frac{\partial x}{\partial \theta} \\ \frac{\partial y}{\partial \theta} \end{pmatrix} = \frac{1}{\sqrt{(-h\varepsilon\, \sin(\theta))^2 + (h\sqrt{\varepsilon^2 - 1}\, \cos(\theta))^2}} \begin{pmatrix} -h\varepsilon\, \sin(\theta) \\ (h\sqrt{\varepsilon^2 - 1}\, \cos(\theta) \end{pmatrix}, \tag{A22}$$

so that

$$\mathbf{e} = \frac{1}{\sqrt{\varepsilon^2 - \cos^2(\theta)}} \begin{pmatrix} -\varepsilon \sin(\theta) \\ \sqrt{\varepsilon^2 - 1}\cos(\theta) \end{pmatrix}. \tag{A23}$$

We now calculate the term $\sin(\phi)$ from the magnitude of the cross-product between **n** and **e**. Thus,

$$\sin(\phi) = |\mathbf{n} \times \mathbf{e}| = \frac{\sqrt{\varepsilon^2 - 1}}{\sqrt{\varepsilon^2 - \cos^2(\theta)}}. \tag{A24}$$

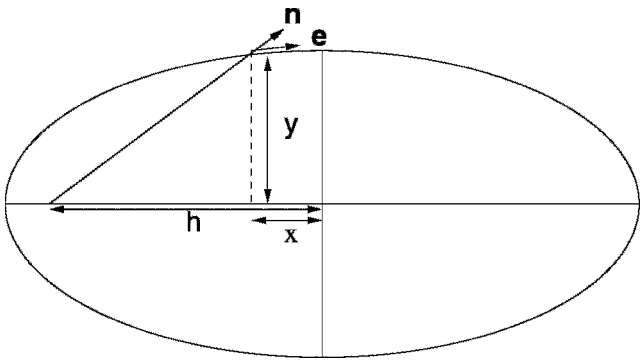

Figure A3. Geometry used to calculate the unit vectors **n** and **e**.

Using $\varepsilon = v_0 t/2h$ we get

$$\sin(\phi) = \frac{\sqrt{\left(\frac{v_0 t}{2h}\right)^2 - 1}}{\sqrt{\left(\frac{v_0 t}{2h}\right)^2 - \cos^2(\theta)}}. \tag{A25}$$

Insert this with eq. (A22) into eq. (A18) and we obtain

$$dA = dx\, dy = h\frac{s}{r_s}\sqrt{\left(\frac{v_0 t}{2h}\right)^2 - 1}\, dl\, d\theta. \tag{A26}$$

From eq. (A26) we can obtain $dl\, d\theta$ as a function of dA. Therefore,

$$dl\, d\theta = \frac{r_s}{s}\frac{dA}{h\sqrt{\left(\frac{v_0 t}{2h}\right)^2 - 1}}, \tag{A27}$$

and we can substitute the integral over dl and $d\theta$ in eq. (A14) with an integral over area, where the area to be integrated is the interior of the single-scattering ellipse at time t, that is,

$$I_s = \frac{1}{2\pi h\sqrt{\left(\frac{v_0 t}{2h}\right)^2 - 1}} \int_A \frac{r_s}{s}(\mathbf{x})\, \delta s(\mathbf{x})\, dA(\mathbf{x}). \tag{A28}$$

By symmetry, the second integral I_g that accounts for the mean traveltime changes of the paths going from the edge of the ellipse to the receiver location **x** gives a similar contribution. Taking the integral I_g into account and using the symmetry of source and receiver location, we get, using the notation of pictured in Fig. 5 the expression for the mean traveltime change for waves in the single-scattering regime with traveltime t

$$\langle \tau(t) \rangle = \frac{1}{2\pi h\sqrt{\left(\frac{v_0 t}{2h}\right)^2 - 1}} \int_A \left[\frac{r_s}{s} + \frac{r_g}{g}\right](\mathbf{x})\, \delta s(\mathbf{x})\, dA(\mathbf{x}). \tag{A29}$$